PAPER

Porous amorphous nitinol synthesized by argon injection: a molecular dynamics study

IOP Publishing Journal of Physics: Condensed Matter
J. Phys.: Condens. Matter **34** (2022) 414003 (7pp) https://doi.org/10.1088/1361-648X/ac8512

Porous amorphous nitinol synthesized by argon injection: a molecular dynamics study

A A Tsygankov[1,*], B N Galimzyanov[1,2] and A V Mokshin[1,2]

[1] Kazan Federal University, 420008 Kazan, Russia
[2] Udmurt Federal Research Center of the Ural Branch of the RAS, 426067 Izhevsk, Russia

E-mail: tsigankov.artiom@gmail.com

Received 24 May 2022, revised 8 July 2022
Accepted for publication 28 July 2022
Published 5 August 2022

Abstract

Porous crystalline nitinol is widely applied in various fields of science and technology due to the unique combination of physical and mechanical properties as well as biocompatibility. Porous amorphous nitinol is characterized by improved mechanical properties compared to its crystalline analogues. Moreover, this material is more promising from the point of view of fundamental study and practical application. The production of porous amorphous nitinol is a difficult task requiring rapid cooling protocol and optimal conditions to form a stable porous structure. In the present work, based on the results of molecular dynamics simulations, we show that porous nitinol with the amorphous matrix can be obtained by injection of argon into a liquid melt followed by rapid cooling of the resulting mixture. We find that the porosity of the system increases exponentially with increasing fraction of injected argon. It has been established that the system should contain about ∼18%–23% argon for obtain an open porous structure, while the system is destroyed by overheated inert gas when the argon fraction is more than ∼23%. It is shown that the method of argon injection makes it possible to obtain a highly porous system with the porosity ∼70% consisting the spongy porous structure similar to aerogels and metallic foams.

Keywords: porous nitinol, argon injection, metallic foams, molecular dynamics, porosity, porous structure

(Some figures may appear in colour only in the online journal)

1. Introduction

Porous titanium nickelide alloy $Ni_{50}Ti_{50}$ known as nitinol is promising due to unique combination of physical and mechanical properties such as open porosity, biocompatibility, shape memory effect and high strength [1, 2]. Therefore, porous nitinol is preferable in medicine, aerospace and transport industries for production of construction details, implants and filter elements [3, 4]. The presence of such properties is largely determined by the crystal structure that supports the austenitic-martensitic (B2→ B19′) and martensitic-austenitic (B19′ →B2) transitions under thermal and mechanical influences [1]. The main advantage of porous crystalline nitinol is the simplicity of its preparation and the availability of initial powder raw materials for synthesis, for example, by powder metallurgy methods [5]. The synthesized porous samples usually have an open porous structure with the average linear size of the pores ∼200 μm, that is close to the pore size in bone tissues [6]. At the same time, porous crystalline nitinol has some limitations, which include increased fragility (with increasing porosity, the fragility also become larger) and the tendency to form cracks [7, 8].

* Author to whom any correspondence should be addressed.

From point of view of fundamental studies and practical applications, porous amorphous nitinol is of great interest [9]. This material is less exposed to crack formation due to the absence of defects, which inevitably occur in the case of the crystalline analogue. It has an increased resistance to external deformations that is confirmed by the results of molecular dynamics simulations. For example, it was shown in [10, 11] that the Young's modulus of porous amorphous nitinol at tensile and compression deformations is more than twice larger then in the case of the crystalline material with the porosity $\phi \in [7.5; 35]\%$. Despite these advantages, it is difficult to synthesize experimentally porous amorphous nitinol. The main reason for this is the need to apply the quench with extremely high rates (more than $1 \times 10^6\,\mathrm{K\,s^{-1}}$) to obtain a stable amorphous structure [12]. Difficulties may also arise at choice an appropriate method for the synthesis of a porous structure. The known methods for preparing porous alloys, such as powder sintering [13], additive technologies [14], spark plasma sintering [4], and self-propagating high-temperature synthesis [15, 16], can lead to formation of a crystalline structure in the powder contact zones [17, 18]. The presence of crystalline inclusions can lead to the degradation in the mechanical characteristics of the porous alloy, for example, due to an increase in the probability of the nanosized cracks formation at the interface between crystal and amorphous phases [19, 20]. Therefore, the method of direct melt foaming by gas injection is the most preferable for obtaining the amorphous structure without crystalline inclusions [21, 22]. This method is widely used to form the pores in various metal melts by gas injection (most often by argon) under high pressure or gas-evolving foaming agents (for example, calcium oxide CaO, titanium hydride TiH_2) or by means of obtaining oversaturated metal-gas solutions followed by cooling the foamed liquid melt. However, this method is difficult to apply for production of porous amorphous nitinol due to the high melting point of $Ni_{50}Ti_{50}$ alloy ($\sim$1570 K) and due to the lack of information about the optimal conditions for foaming the corresponding melt. Insufficient understanding of the pore formation mechanisms in the nitinol melt requires detailed studies related to molecular dynamics simulations.

In the present work, the process of liquid nitinol foaming via argon injection is studied by means of molecular dynamics simulations. The simulation conditions are close to the experimental ones implemented, for example, in the method of direct melt foaming by gas injection [21, 22]. We determine the optimal fraction of the injected argon and the thermodynamic parameters of the system to obtain the porous amorphous alloy with the required porosity and the required pore morphology. The possibility of obtaining porous amorphous nitinol with closed pores (porosity up to 35%) and with an open percolating porous structure (with porosity up to 70%) is demonstrated. In section 2, the melt foaming procedure and the details of the applied hybrid interparticle interaction potential are discussed. Section 3 is devoted to discussion of the obtained results. The conclusion is given in section 4.

2. Argon injection procedure

Initially, crystalline nitinol consisting 68 750 atoms of Ni and 68 750 atoms of Ti was chosen. Molecular dynamics simulations are performed in the isobaric-isothermal (NPT) ensemble with the time step 1 fs using the Lammps simulation package [23]. At all stages of the simulations, the pressure is equal to 1 atm.

The interaction between Ni, Ti and Ar atoms is specified using the hybrid interaction potential. For Ni–Ni, Ti–Ti and Ni–Ti interactions, the 2NN MEAM potential is applied to compute the total energy of the system [24]:

$$E = \sum_{i=1}^{N} \left[F_i(\rho_i) + \frac{1}{2} \sum_{j \neq i}^{N} S_{ij} \phi_{ij}(r_{ij}) \right]. \tag{1}$$

Here, F_i is the embedding function for the atom i within a background electron density ρ_i; the pair potential $\phi_{ij}(r_{ij})$ and screening function S_{ij} are evaluated at the distance r_{ij} between atoms i and j. In the 2NN MEAM potential, the pairwise interaction $\phi_{ij}(r_{ij})$ is not assigned a simple functional expression. As a rule, the value of the quantity $\phi_{ij}(r_{ij})$ is estimated by the embedding energy and the energy per atom

$$\phi_{ij}(r_{ij}) = \frac{2}{Z_1} \left\{ E_i^u(r_{ij}) - F_i(\rho_i) \right\}. \tag{2}$$

In equation (2), Z_1 is the number of nearest-neighbor atoms, $E_i^u(r_{ij})$ is the energy per atom [25]:

$$E_i^u(r_{ij}) = -E_c(1 + a^* + da^{*3})\mathrm{e}^{-a^*}, \tag{3}$$

where

$$a^* = \sqrt{\frac{9B\Omega}{E_c}} \left(\frac{r_{ij}}{r_e} - 1 \right). \tag{4}$$

Here, r_e is the equilibrium nearest-neighbor distance; E_c is the cohesive energy; d is an adjustable parameter; B is the bulk modulus; Ω is the equilibrium atomic volume of the reference structure. The values of these parameters for Ni–Ti system are given in table IV of [24]. The cutoff radius of the 2NN MEAM potential is 5.0 Å for considered binary system. For Ni–Ar, Ti–Ar and Ar–Ar interactions, the binary Lennard-Jones potential is applied [26]:

$$E_{LJ}(r_{ij}) = 4\epsilon_{\alpha\beta} \left[\left(\frac{\sigma_{\alpha\beta}}{r_{ij}} \right)^{12} - \left(\frac{\sigma_{\alpha\beta}}{r_{ij}} \right)^{6} \right], \alpha, \beta = \{\mathrm{Ni}, \mathrm{Ti}, \mathrm{Ar}\}. \tag{5}$$

The parameters of this potential—the potential well depth $\epsilon_{\alpha\beta}$ and the effective atom diameter $\sigma_{\alpha\beta}$—are given as follows: $\epsilon_{\mathrm{ArTi}} = 8.7 \times 10^{-2}$ eV and $\sigma_{\mathrm{ArTi}} = 3$ Å for Ar–Ti interaction; $\epsilon_{\mathrm{ArNi}} = 7.9 \times 10^{-2}$ eV and $\sigma_{\mathrm{ArNi}} = 3.04$ Å for Ar–Ni; $\epsilon_{\mathrm{ArAr}} = 1 \times 10^{-2}$ eV and $\sigma_{\mathrm{ArAr}} = 3.41$ Å for Ar–Ar [27]. The applied cutoff radius of the Lennard-Jones potential is $2.5\sigma_{\alpha\beta}$.

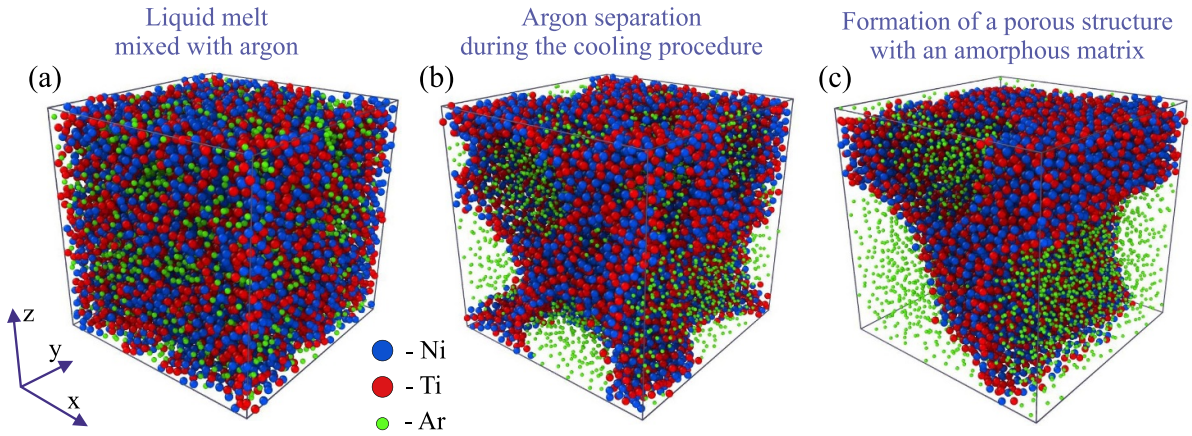

Figure 1. Snapshots of the system in various states: (a) liquid melt mixed with argon; (b) redistributed Ni, Ti and Ar atoms at the stage of cooling of the liquid melt; (c) porous structure and amorphous matrix upon cooling of the liquid melt with injected argon.

The argon injection procedure and the preparation of porous amorphous nitinol are carried out through the following steps:

- The liquid sample is melted at the temperature $T = 1.2T_m$, where the melting temperature is $T_m \simeq 1570$ K, and, then, it is brought to the thermodynamic equilibrium state during the time 0.1 ns.
- The injection of Ar atoms is carried out. This procedure means the random replacement of some Ni and Ti atoms by Ar atoms (see figure 1(a)). Here, the proportion of Ni and Ti atoms in the system always remains the same and corresponds to $Ni_{50}Ti_{50}$ alloy. The liquid samples are prepared by injection of argon in the fractions $f = 10$, 14, 15, 16, 17, 18, 19, 20 and 23% from the total number of atoms in the system. After the injection of argon, the system is again brought to the thermodynamic equilibrium state.
- The liquid nitinol mixed with argon is rapidly cooled to the temperature 300 K at the cooling rate 1×10^{12} K s^{-1}. The redistribution of the components occurs during the cooling procedure, as a result of which argon is separated from amorphous nitinol (see figures 1(b) and(c)). The separation of argon gas and solid nitinol occurs heterogeneously. This leads to the formation of the foamed amorphous samples, where the percolating network of pores filled with argon. Note that the porosity and distribution of pores in the system may be dependent on the cooling rate applied to generate the porous amorphous system [28, 29].
- The foamed samples were held at the temperature 300 K for the time 0.1 ns for stabilization of the amorphous matrix. Then, argon is completely removed from the system. The resulting porous amorphous samples are held again at the temperature 300 K.

The porosity ϕ of the obtained samples is determined by the well-known expression [30]:

$$\phi = \left(1 - \frac{\rho}{\rho_0}\right) \cdot 100\%, \tag{6}$$

where ρ is the density of a porous sample, $\rho_0 = 6.21$ g cm^{-3} is the density of nitinol without pores at the temperature $T = 300$ K.

To avoid the artifacts due to the molecular dynamics simulations of a porous system, the following condition must be satisfied: the average linear pore size must be less than the linear size of the simulation box. In this case, there will be no significant artifacts generated by the periodic boundary conditions. In the present study, the linear size of the simulated system is set so that it exceeds the characteristic size of the pores formed in the system. For example, in the case of the porosity 25%, the linear size of the system is $L \approx 14.8$ nm, while the average linear pore size is $l \approx 3$ nm. In the case of the maximum considered porosity 70%, we have $L \approx 26$ nm and $l \approx 20$ nm.

3. Porosity as function of Argon fraction

Figure 2 shows the dependence of the porosity ϕ on the injected argon fraction f. We find that porous amorphous nitinol contains only closed pores at argon less than ∼18%. In this case, the system porosity does not exceed $\phi = 35\%$. The resulting pores are stable and have a shape close to spherical. Average linear size of the closed pores is ∼2 nm, which is a low threshold value for porous alloys belonging to the class of nanoporous materials [31]. To obtain the porous structure with open pores and the percolating amorphous matrix, the fraction of argon must be above 18%. Here, the argon fraction from f ∼18% to 23% is optimal. In this case, the porosity of the system varies in the range $\phi \in [40; 70]\%$. It is important to note that the fraction of the injected argon should not exceed ∼23%–25% at the considered thermodynamic conditions. The structure of the system is destroyed with an increase in the argon fraction above this value: the liquid melt is decayed by overheated argon. Thus, the optimal fraction of the injected argon required to obtain the highly porosity system with open pores is about ∼20% at the considered thermodynamic conditions.

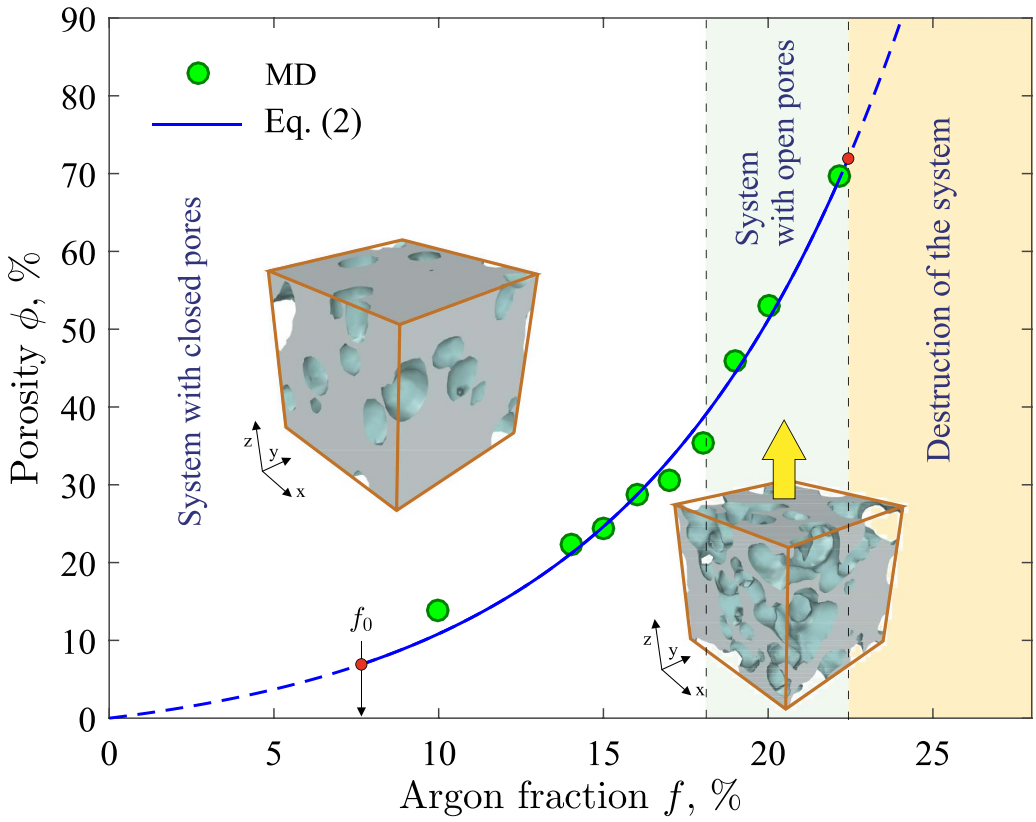

Figure 2. Dependence of the porosity ϕ on the injected argon fraction f. Regions corresponding to the amorphous system with different porous structures (with open pores, with closed pores) are identified. The system instability region is shown, where the addition of Ar atoms leads to the destruction of the system.

We find that the dependence of the system porosity on the injected argon fraction can be reproduced by the exponential law

$$\phi(f) = \phi_0 \left[e^{f/f_0} - 1 \right], \ f \geqslant f_0. \tag{7}$$

Here, ϕ_0 is the fraction of the free volume in the system without pores; this parameter is related to the packing fraction f_p, $\phi_0 \approx 1 - f_p$ [32, 33]. The parameter f_0 characterizes the minimum fraction of the injected argon that is sufficient for the formation of stable pores. Expression (7) is an empirical result and it is realized at $f \geqslant f_0$. In fact, equation (7) indicates that the density of the porous system ρ is related to the fraction of injected gas f according to the exponential law

$$\rho(f) = \rho_0(1 + \phi_0 - \phi_0 e^{f/f_0}), \ f \geqslant f_0. \tag{8}$$

Both equations (7) and (8) take into account the physical effect associated with the fact that there is a minimum fraction of injected gas f_0, at which stable pores are formed in the system and the system is not able to 'heal' these pores. The values of the parameters f_0 and ϕ_0 were determined by fit of equation (7) to the simulation data. For the considered system, the found value $f_0 = (7.6 \pm 0.8)\%$ determines the minimum argon fraction that should be injected into nitinol melt to obtain the minimum porosity $\phi(f_0) \approx 1.72\phi_0 \approx 6.9\%$, where $\phi_0 = (4.0 \pm 1.0)\%$. The formed pores will coalesce after removal of Ar atoms from the system if value of the parameter f_0 is less than 7.6%. We find that for the case minimal porosity with $\phi(f_0)$ it is satisfied the correlation relation $f_0 \approx 1.9\phi_0$. Then, from expression (8) at $f = f_0$ we find

$$\rho(f_0) \approx \rho_0(1 - 0.9f_0). \tag{9}$$

Expression (9) shows the ultimate density of the system, at which the formation of stable pores becomes possible.

Figure 3 shows the fragment of the amorphous matrix of porous nitinol with the porosity 70%. As can be seen from this figure, the so-called spongy porous structure is formed at injected of more than 20% argon. The reason for formation of such spongy structure is the thermal expansion of the liquid melt due to the large fraction of overheated noble gas. In this spongy porous structure the average thickness of the interpore walls is much less than the average linear size of the pores: average thickness of interpore walls is ~5 nm, while the average linear size of the pores is ~20 nm. We note that nitinol is in the state of viscous liquid at the considered temperature ≃1890 K, while argon at this temperature is in strongly overheated gas phase (the melting temperature of solid argon is ~88 K). Despite the high fraction of argon, the high viscosity of liquid nitinol does not allow the gas phase to be completely separated from the melt. Thus, the partial coalescence of the formed gas bubbles and foaming of liquid nitinol are occurred. The high viscosity of the melt also contributes to

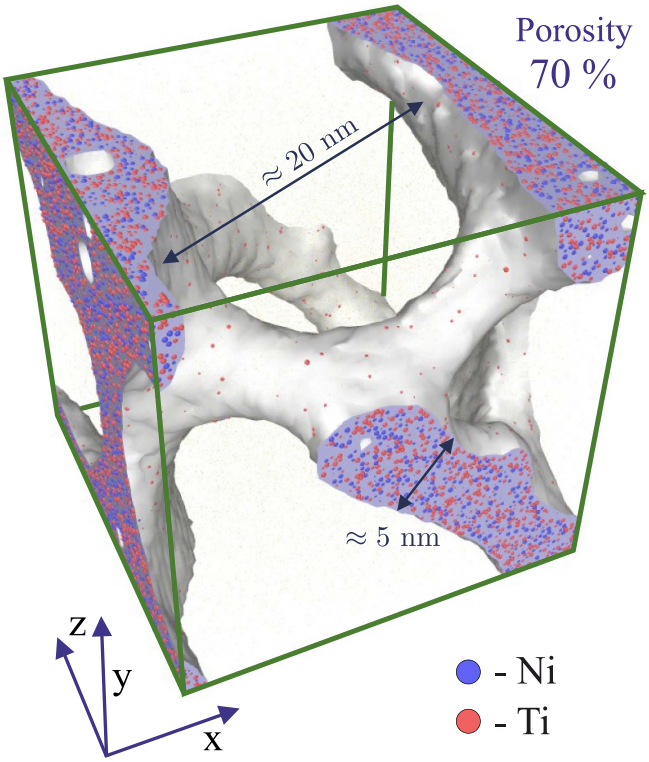

Figure 3. Snapshot of the system with porosity ∼70% prepared by injecting 23% argon.

formation of the percolating matrix at the cooling procedure (see figure 3). It is noteworthy that such the spongy porous structure almost completely corresponds to the structure of organic foams, aerogels and metallic foams, the porosity of which ones usually is larger than 70% [34–38]. Average value of the linear size of the pores in the considered system is also close to the pore size in aerogels, where pores can have sizes from ∼10 to ∼100 nm [39]. Such the spongy porous structure could be of great interest for various practical applications: for example, for the design of filter elements, fuel reservoirs and battery electrodes [40].

4. Conclusion

Based on the results of molecular dynamics simulations, we have shown the possibility of obtaining porous amorphous nitinol by injecting argon into the corresponding melt. The energies and forces between Ni, Ti, and Ar atoms were correctly calculated using the hybrid interparticle interaction potential, which made it possible to obtain the porous system whose structure is close to experimentally synthesized aerogels and metallic foams. A relationship between the fraction of the injected argon and the system porosity has been determined, which is well reproduced by an exponential function. We have determined the optimal fraction of the injected argon, which makes it possible to obtain the porous amorphous nitinol with the spongy structure and with the stable amorphous matrix without crystalline inclusions. The limiting fraction of the injected argon was also found, the excess of which leads to the complete extrusion of argon from the liquid melt and to destroy of the system. It is shown that for formation of stable porous structure, the minimum fraction of the injected argon should not be less than ∼7.6% at the considered thermodynamic conditions. The obtained results show that well-known method of direct melt foaming by gas injection [21, 22] can be adapted for the synthesis of porous amorphous nitinol if the rapid cooling protocol will be implemented.

The results of the present study are practically significant and can be applied to improve the foaming protocols of metal melts. For example, based on the results presented in figure 2, it is possible to determine the optimal ratio of foaming gas and metal melt to obtain a sample with the required porosity and pore morphology. This makes it possible to simplify the procedure for synthesizing samples with desired mechanical properties for specific applications, for example, for the manufacture of construction materials or implants [41, 42]. Moreover, the ultimate value of the argon fraction necessary to obtain a highly porous system with the porosity ∼70% was determined for the first time. At such porosity, we have a sponge-like porous structure as in the case of aerogels, organic and metal foams. This result is of great importance in production of porous filters and biocompatible porous nanoparticles, for example, for the delivery and storage of drugs in humans [43–45].

Data availability statement

All data that support the findings of this study are included within the article (and any supplementary files).

Acknowledgments

The work was supported by the Russian Science Foundation (Project No. 19-12-00022-P). A V M is grateful to the Foundation for the Development of Theoretical Physics and Mathematics ‘Basis’, which contains part of the work related to the implementation of theoretical calculations. The review part about properties of perspective materials is supported by the Kazan Federal University Strategic Academic Leadership Program (PRIORITY-2030).

ORCID iDs

A A Tsygankov https://orcid.org/0000-0002-0614-5361
B N Galimzyanov https://orcid.org/0000-0002-1160-5748
A V Mokshin https://orcid.org/0000-0003-2919-864X

References

[1] Kapoor D 2017 Nitinol for medical applications: a brief introduction to the properties and processing of nickel titanium shape memory alloys and their use in stents *Johnson Matthey Technol. Rev.* **61** 66–76

[2] Ishizaki K, Komareni S and Nanko M 1998 Applications of porous materials *Porous Materials* (Boston, MA: Springer)

[3] Chaudhari R, Vora J J and Parikh D M 2020 *Recent Advances in Mechanical Infrastructure Proceedings of ICRAM 2020* (Berlin: Springer)

[4] Bansiddhi A, Sargeant T D, Stupp S I and Dunand D C 2011 Porous NiTi for bone implants: a review *Acta Biomater.* **4** 773–82

[5] Yasenchuk Y 2019 Biocompatibility and clinical application of porous TiNi alloys made by self-propagating high-temperature synthesis (SHS) *Materials* **12** 2405

[6] Augat P and Schorlemmer S 2006 The role of cortical bone and its microstructure in bone strength *Age Ageing* **35** ii27–ii31

[7] Bosingnore C 2017 Present and future approaches to lifetime prediction of superelastic nitinol *Theor. Appl. Fract. Mech.* **92** 298–305

[8] Nakas G I, Asik E E, Tunca B and Bor S 2014 Fatigue and fracture behavior of porous TiNi alloys *THERMEC 2013: Int. Conf. on Processing and Manufacturing of Advanced Materials: Processing, Fabrication, Properties, Applications (Las Vegas, USA, 2–6 December, 2013)* vol 783, ed B Mishra, M Ionescu and T Chandra (Durnten-Zurich: Trans Tech Publications Ltd)

[9] Gunther V *et al* 2019 Formation of pores and amorphous-nanocrystalline phases in porous TiNi alloys made by self-propagating high-temperature synthesis (SHS) *Adv. Powder Technol.* **4** 673–80

[10] Galimzyanov B N and Mokshin A V 2021 Mechanical response of mesoporous amorphous NiTi alloy to external deformations *Int. J. Solids Struct.* **224** 111047

[11] Panico M and Brinson L C 2008 Computational modeling of porous shape memory alloys *Int. J. Solids Struct.* **45** 5613–26

[12] Galimzyanov B N and Mokshin A V 2020 Amorphous porous phase of nitinol generated by ultrafast isobaric cooling *Solid State Phenom.* **310** 150–5

[13] Anikeev S, Yakovlev E, Artyukova N, Mamazakirov O, Kaftaranova M and Promakhov V 2020 *2020 7th Int. Congress on Energy Fluxes and Radiation Effects* (*EFRE*)

[14] Karaji J Z, Speirs M, Dadbak S, Kruth J-P, Weinans H, Zadpoor A A and Yavari S A 2016 Additively manufactured and surface biofunctionalized porous nitinol *ACS Appl. Mater. Interfaces* **9** 1293–304

[15] Shiskovski I 2012 Hysteresis modeling of the porous nitinol delivery system, designed and fabricated by SLS method *Phys. Proc.* **39** 893–902

[16] Biswas A 2005 Porous NiTi by thermal explosion mode of SHS: processing, mechanism and generation of single phase microstructure *Acta Mater.* **53** 1415–25

[17] Galimzyanov B N, Yarullin D T and Mokshin A V 2018 Change in the crystallization features of supercooled liquid metal with an increase in the supercooling level *JETP Lett.* **107** 629–34

[18] Galimzyanov B N, Nikiforov G A and Mokshin A V 2020 Effect of ultrafast cooling on pore formation in amorphous titanium nickelide *Acta Phys. Pol.* A **137** 1149–52

[19] Jiang S, Tang M, Zhao Y, Hu L, Zhang Y and Liang Y 2013 Crystallization of amorphous NiTi shape memory alloy fabricated by severe plastic deformation *Trans. Nonferr. Met. Soc. China* **24** 1758–65

[20] Galimzyanov B N and Mokshin A V 2018 Morphology of critically sized crystalline nuclei at shear-induced crystal nucleation in amorphous solid *J. Rheol.* **62** 265–75

[21] Banhart J 2001 Manufacture, characterisation and application of cellular metals and metal foams *Prog. Mater. Sci.* **46** 559–632

[22] Brothers A H and Dunand D C 2006 Amorphous metal foams *Scr. Mater.* **54** 513–20

[23] Thompson A P *et al* 2022 LAMMPS—a flexible simulation tool for particle-based materials modeling at the atomic, meso and continuum scales *Compt. Phys. Commun.* **271** 108171

[24] Ko W S, Grabowski B and Neugebauer J 2015 Development and application of a Ni-Ti interatomic potential with high predictive accuracy of the martensitic phase transition *Phys. Rev.* B **92** 134107

[25] Lee B-J and Baskes M I 2000 Second nearest-neighbor modified embedded-atom-method potential *Phys. Rev.* B **62** 8564

[26] Daun K J, Titantah J T and Karttunen M 2012 Molecular dynamics simulation of thermal accommodation coefficients for laser-induced incandescence sizing of nickel particles *Appl. Phys.* B **107** 221–8

[27] Hansen J-P and Verlet L 1969 Phase transitions of the Lennard-Jones system *Phys. Rev.* **184** 151–61

[28] Nagaumi H 2001 Prediction of porosity contents and examination of porosity formation in Al-4.4% Mg DC slab *Sci. Technol. Adv. Mater.* **2** 49–57

[29] Carlson K D, Lin Z and Beckermann C 2007 Modeling the effect of finite-rate hydrogen diffusion on porosity formation in aluminum alloys *Metall. Mater. Trans.* B **38** 541–55

[30] Flint E L and Flint A L 2002 Porosity *Methods of Soil Analysis, Part 4: Physical Methods* (Hoboken, NJ: Soil Science Society of America, Inc.) ch 2.3

[31] Mishra R, Militky J and Venkataraman M 2019 Nanoporous materials *Nanotechnology in Textiles: Theory and Application* (Cambridge: Woodhead Publishing) ch 7

[32] Kittel C 2005 *Introduction to Solid State Physics* (Hoboken, NJ: Wiley)

[33] Filion L and Dijkstra M 2009 Prediction of binary hard-sphere crystal structures *Phys. Rev.* E **79** 046714

[34] Bhattacharya A, Calmidi V V and Mahajan R L 2002 Thermophysical properties of high porosity metal foams *Int. J. Heat Mass Transfer* **45** 1017–31

[35] Sehaqui H, Zhou Q and Berglund A L 2011 High-porosity aerogels of high specific surface area prepared from nanofibrillated cellulose (NFC) *Compos. Sci. Technol.* **71** 1593–9

[36] Qiu L, Yan K, Feng Y, Liu X and Zhang X 2021 Bionic hierarchical porous aluminum nitride ceramic composite phase change material with excellent heat transfer and storage performance *Compos. Commun.* **27** 100892

[37] Qiu L, Du Y, Bai Y, Feng Y, Zhang Z, Wu J, Wang X and Xu C 2021 Experimental characterization and model verification of thermal conductivity from mesoporous to macroporous SiOC ceramics *J. Therm. Sci.* **30** 465–76

[38] Qiu L, Zou H, Tang D, Wen D, Feng Y and Zhang Z 2018 Inhomogeneity in pore size appreciably lowering thermal conductivity for porous thermal insulators *Appl. Therm. Eng.* **130** 1004–11

[39] Daero L, Jinyoung K, Seohyun K, Gunhwi K, Jihun R, Sangrae L and Haksoo H 2019 Tunable pore size and porosity of spherical polyimide aerogel by introducing swelling method based on spherulitic formation mechanism *Microporous Mesoporous Mater.* **288** 109546

[40] Liu P S and Chen G F 2014 Application of porous metals *Porous Metals* (Beijing: Tsinghua University Press Limited)

[41] Prasad K *et al* 2017 Metallic biomaterials: current challenges and opportunities *Materials* **10** 884

[42] Aihara H, Zider J, Fanton G and Duerig T 2019 Combustion synthesis porous nitinol for biomedical applications *Int. J. Biomater.* **2019** 4307461
[43] Malloy J, Quintana A, Jensen C J and Liu K 2021 Efficient and robust metallic nanowire foams for deep submicrometer particulate filtration *Nano Lett.* **21** 2968–74
[44] Parra-Nieto J, Cid M, Carcer I and Baeza A 2020 Inorganic porous nanoparticles for drug delivery in antitumoral therapy *Biotechnol. J.* **16** 2000150
[45] Zhou M, Shen L, Lin X, Hong Y and Feng Y 2017 Design and pharmaceutical applications of porous particles *RSC Adv.* **7** 39490–501